Influence of ordering phenomena on carbon segregation in tungsten screw dislocation

Fabienne Berthier, Bernard Legrand

Acta Materialia 245 (2023) 118610

Contents lists available at ScienceDirect

Acta Materialia

journal homepage: www.elsevier.com/locate/actamat

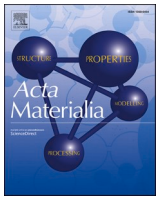

Influence of ordering phenomena on carbon segregation in tungsten screw dislocation

F. Berthier [a,*], B. Legrand [b]

[a] Université Paris-Saclay, CNRS, Institut de chimie moléculaire et des matériaux d'Orsay, Orsay 91405, France
[b] Université Paris-Saclay, CEA, Service de Métallurgie Physique, Gif-sur-Yvette 91191, France

ARTICLE INFO

Keywords:
Segregation
Short-range ordering
Long-range ordering
Carbon
Screw dislocation

ABSTRACT

Concentration profiles on the different sites of tungsten screw dislocation are calculated as a function of the nominal carbon atom concentration, temperature and dislocation density. Rigid lattice Monte Carlo simulations and associated mean-field modelling are performed based on interaction energies from *ab initio* calculations. We show that the repulsive interactions induce ordering phenomena that drastically change the concentration in the core of the dislocation and leads to ordered structures among the octahedral sites. We detail the domains of short-range ordering (SRO) and long-range ordering (LRO).

1. Introduction

The chemical composition at interfaces (dislocation, grain boundaries), surfaces, thin films and nanoparticles often differs from that of the bulk. This so-called segregation phenomenon is of great importance for the physical and chemical properties of materials. For dislocations, segregation can have an important mechanical influence via the variation of their mobility according to the concentration of the segregating element [1].

Segregation is very well documented, both from the experimental and from the theoretical point of view. At the atomic scale, it has already been possible to characterize surface segregation with STM [2,3], while for dislocations HREM [4], ToF-FIM [5] and three-dimensional atomic probe (ATP) [6–8] can lead to atomic resolution. Theoretically, intensive research has been devoted for segregation at surfaces and thin films [9–12], grain-boundaries [13–16], nanoparticles [17–21] and nanowires [22]. For dislocations, the segregation was modeled either using elastic theory [23–27], or using Monte-Carlo simulations with semi-empirical potentials [28–31], or using *ab initio* calculations whose obtained interactions are used as input data in rigid-lattice MC simulations or mean field models [32–34]. The goal is then to obtain the equilibrium concentration of the segregating elements in the core of the dislocations as a function of their bulk concentration, temperature and dislocation density.

On the surface, the coupling between segregation and order phenomena [35] has been extensively studied, this coupling being likely to largely modify the surface segregation [3,9,36–40]. This coupling has also been studied for intergranular segregation [13,14,41,42] and in thin films and nanoparticles [17,18,43–52]. It seems that the same theoretical effort has not been carried out on this coupling for segregation in the core of dislocations [33,34]. The fact that there is no phase transition at 1D [53] can perhaps explain this relative lack of interest in studying this coupling for dislocations.

The aim of this paper is to show that taking into account the coupling between order and segregation phenomena in the case of dislocations is as important as for interfaces and nanoparticles. The order phenomena can be both long-range order (LRO) and short-range order (SRO) and affect the bulk or the core of dislocations.

We consider the segregation of carbon in the core of $1/2\ \langle 111 \rangle$ screw dislocation in tungsten. The interactions between carbon atoms are obtained by *ab initio* calculations [33] and are input into Monte Carlo simulations and into a mean-field model allowing the emergence of order phenomena. The comparison with a previous study in which only the disordered state was allowed in the core of the dislocation [33] allows to highlight the importance of the coupling between segregation and order phenomena in the core of dislocations.

The paper is organized as follows. After the description of the energetic model in Section 2, we present the computational methods (Section 3), including in particular the description of the mean-field model which takes into account the possible ordering phenomena. Section 4 details results obtained with mean-field modelling and presents a comparison with the Monte Carlo results. Finally, we discuss the main

* Corresponding author.
E-mail address: fabienne.berthier@universite-paris-saclay.fr (F. Berthier).

https://doi.org/10.1016/j.actamat.2022.118610
Received 11 October 2022; Received in revised form 30 November 2022; Accepted 10 December 2022
Available online 11 December 2022

features of the thermodynamics of the considered system, in particular the ordering phenomena (Section 5), before concluding (section 6).

2. Energetic parameters

We consider the energetic model of the original work [33] which was determined from *ab initio* calculations. The energy of the reconstructed dislocation is given by an Ising Hamiltonian:

$$H = H_0 + \sum_i \Delta E_i^{seg,0} \sigma_i + \sum_{i,j \neq i} V_{ij} \sigma_i \sigma_j. \quad (1)$$

The Hamiltonian depends on two elements, the segregation energies $\Delta E_i^{seg,0}$ in dilute limit on site i and the pair interaction energies V_{ij} between carbon atoms on two sites i and j. Both the prismatic P sites inside the dislocation core and the six different $O^{(4)}$ sites around the reconstructed core are taken into account (see Fig. 1a). In the following, in order to simplify the notations, the octahedral lines $O^{(4)}$ are named O. H_0 is a constant term, proportional to the energetic cost to transform a dislocation segment from an easy to a hard core. σ_i is an occupation number, which equals 1 if the site i is occupied by an atom, and 0 otherwise. The interactions between atoms are restricted to the nearest neighbor sites.

The segregation energy is the energy variation in dilute limit between an initial configuration and a final configuration where a carbon atom is respectively located in a site of the bulk and in a site on the dislocation. The segregation energies on sites P (in the hard configuration induced to the carbon segregation) and on sites O are respectively equals to $\Delta E_P^{seg,0} = -2.1$ eV and $\Delta E_O^{seg,0} = -1.38$ eV. The segregation energy is twice higher (in absolute value) on P sites than on O sites. That means that carbon segregation is strongly favored in the P line. This difference in segregation energy may be related to steric effects. It would be interesting to extend the analysis of the driving forces of segregation that is performed at the surface and at grain boundaries in metal alloys [15,54] to dislocations for metal-carbon systems.

The intra-line interaction energies, *i.e.* the interaction energies between two carbon atoms belonging to the same line P or O are respectively $V_{PP} = -0.08$ eV and $V_{OO} = -0.27$ eV (see Fig. 1b). These interactions are attractive. The system tends to phase separation along the P and O lines. The intra-line interaction on the P line is weak (almost nil) and strong on the O line. Intra-line phase separation can therefore be expected on line P and especially on line O.

All the inter-line interactions are repulsive: $V_{PO} = 0.06$ eV, $V_1 = 0.25$ eV, $V_2 = 0.61$ eV, $V_3 = 0.18$ eV and $V_4 = 0.13$ eV (see Figs. 1a and 1b). The tendency of chemical order between the P line and O lines is weak and strong between two neighboring O lines. Therefore, the possibility of observing ordered inter-O-line structures cannot be excluded.

3. Computational methods

Based on the attractive intra-line and repulsive inter-line interaction energies, the system may present ordered structures and simulations have to allow this complexity.

3.1. Monte Carlo simulations

We perform Metropolis MC simulations in the grand canonical ensemble, which enables the optimization of both the number and distribution of the carbon atoms on the different sites. Only one type of event is included. Incorporation and extraction of carbon atoms are proposed. A site is chosen randomly. If the site is empty then the incorporation of a carbon atom is proposed, otherwise extraction is proposed. A trial is accepted/rejected following the Metropolis algorithm [55]. The probabilities of incorporation and extraction are respectively:

$$P_I = \frac{N}{N_C + 1} \exp\left(- \frac{\Delta E_I - \mu}{k_B T} \right) \text{ and } P_E = \frac{N_C}{N} \exp\left(- \frac{\Delta E_E - \mu}{k_B T} \right) \quad (2)$$

with N the number of sites and N_C the number of carbon atoms in the cell. ΔE_I (respectively ΔE_E) represents the energy variation due to the incorporation (resp. extraction) of a carbon atom. Each energy is given by the Hamiltonian (Eq. 1) which depends on the configuration via the site occupation numbers. μ is the chemical potential which is calculated from the mean-field formalism in dilute limit:

$$\mu = E_0 + k_B T \ln \frac{c_{bulk}}{1 - c_{bulk}} \quad (3)$$

where E_0 is the incorporation energy of one isolated carbon atom into a bulk octahedral site and c_{bulk} the concentration of carbon. Interaction between carbon atoms in the bulk are neglected which is available for bulk concentrations lower than 1000 appm as considered here. The bulk solubility limit should also be considered especially when $T \to 0$ K. According to the experimental phase diagram, the solubility limit is less than 0.3 % (3000 appm) [56].

MC simulations allow the determination of isotherms and isoconcentrations, *i.e.* the evolution of the concentration of the dislocation sites as a function of the chemical potential (or as a function of the bulk concentration) at a given temperature and respectively as a function of temperature for a fixed value of the bulk concentration.

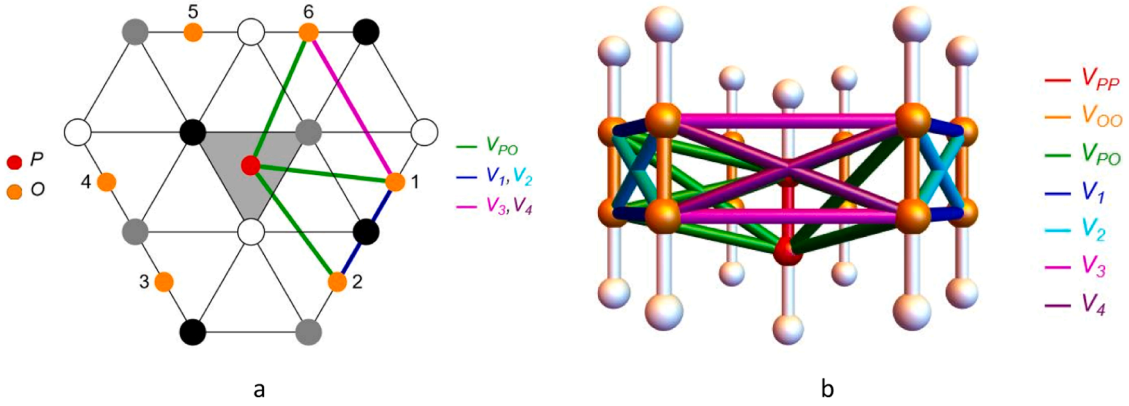

Fig. 1. Schematic representation of the alloying pair interactions between P and O sites: (a) projection on the (111) plane and (b) in projection along the Burgers vector direction. The tungsten atoms are represented in white, black and grey (a); the reconstructed dislocation core is displayed by a grey triangle (a) and carbon atoms are in color (a and b). The prismatic site P inside the hard core is depicted in red while the O_k sites, with k ranging from 1 to 6, are in orange. The interaction terms V_{PP}, V_{PO}, V_{OO}, V_1, V_2, V_3 and V_4 are plotted in red, dark green, orange, blue, cyan, pink and purple, respectively. (For interpretation of the references to colour in this figure legend, the reader is referred to the web version of this article.)

The simulation box contains the line of prismatic P sites and the six lines of octahedral O sites. Each line is composed of $l_d = 100$ sites. The total number of sites is $N = 700$ and the number of MC macro steps is $N_{MC} = 10^6$. Periodic boundary conditions are used. Hereafter we will not present the concentrations per site but the concentrations of lines $c_X = \frac{1}{N_{MC}} \sum_{N_{MC}} \frac{1}{l_d} \sum_{n=1}^{l_d} \sigma_n$, with σ_n the occupation number and $X = P$ or O_i, with $i = 1, \ldots, 6$.

In addition, we calculate the Warren-Cowley short-range order parameter (SRO):

$$\alpha_{XY} = 1 - l_d \frac{N_{C_X E_Y}}{Z_{XY} N_{C_X} (l_d - N_{C_X})} \tag{4}$$

with $X, Y = P$ or O_i, $i = 1, \ldots, 6$; $N_{C_X E_Y}$ the number of first neighboring pairs with a carbon atom (C) on line X and an empty site (E) on line Y; N_{C_X} the number of carbon atom (C) on line X and Z_{XY} the inter-line $X-Y$ coordination number.

3.2. Mean-field modelling

We also perform mean-field calculations which allow a detailed analysis of results. The great advantage of MF modelling is to explore exhaustively all the concentration profiles that are solutions of the system. Given the repulsive interactions between the O lines and thus the possibility that the system forms an ordered inter-O-line structure we have considered the P line and two O lines (lines 1 and 2 for example, see Fig. 1a). We have verified that the results are identical to those of a more complete model including the P-line and the six O lines or even the with per-site formalism.

Using the Bragg-Williams approximation, the minimization of the free energy leads to the well-known segregation equation:

$$\frac{c_X}{1 - c_X} = \frac{c_{bulk}}{1 - c_{bulk}} exp\left(- \frac{\Delta E_X^{seg}}{k_B T} \right), \tag{5}$$

With $X = P$ for the P line and $X = 1, 2$ respectively for the O_1 and O_2 lines. ΔE_X^{seg} the segregation energy in the X line:

$$\Delta E_P^{seg} = \Delta E_P^{seg,0} + 2\ V_{PP} c_P + 6\ V_{PO}(c_1 + c_2), \tag{6a}$$

$$\Delta E_{O_1}^{seg} = \Delta E_O^{seg,0} + 2\ V_{PO} c_P + 2\ V_{OO} c_1 + V_{1-2} c_2, \tag{6b}$$

$$\Delta E_{O_2}^{seg} = \Delta E_O^{seg,0} + 2\ V_{PO} c_P + 2\ V_{OO} c_2 + V_{1-2} c_1. \tag{6c}$$

The total inter-O-line interaction energy $V_{1-2} = V_1 + 2V_2 + V_3 + 2V_4 = 1.91$ eV is very high, which strengthens the assumption of an inter-O-line ordering. Such order is characterized by the long-range order parameter (LRO) $\eta = c_1 - c_2$, which implies describing the two O-lines separately. A mean-field model with a single O-line, *i.e.* that assumes a homogeneous distribution on all O-lines, cannot account for an inter O-line order.

Solving Eq. 5 gives the carbon concentration on the different lines for an isolated dislocation. To take into account the dislocation density ρ, we consider the conservation of matter that relates the bulk carbon concentration to the nominal concentration, without taking into account their relative position and the interactions between them, as following $\frac{N_{bulk}}{3}\ c_{nom} = N_{bulk} c_{bulk} + N_P\ c_P + N_O \sum_i c_{O_i}$ with $N_{bulk} = \frac{6V}{a^3}$, $N_P = \frac{\rho V}{b}$ and $N_O = N_P$ for a volume V with a lattice parameter a and the dislocation burgers vector b. After simplification, with the notations defined above, this relationship becomes:

$$c_{nom} = 3c_{bulk} + 3\rho \frac{a^3}{6b} (c_P + 3\ (c_1 + c_2)). \tag{7}$$

4. Results

If MC simulations are a very efficient method to characterize the segregation phenomena, the SRO and LRO, it is only a numerical method. The mean-field modelling has the advantage to be analytical, which permits an easy analysis of the thermodynamic driving forces. Moreover, we can quickly test the whole range of temperature and concentration. Therefore, we first present the mean-field results, and complete the study by comparison with MC.

4.1. Isotherms

In Fig. 2, the segregation isotherms are shown at $T = 2000$ K, giving the concentration of the three lines $P, O_1, O_2 : c_P, c_1$ and c_2, as a function of the bulk concentration c_{bulk}. As the segregation energy on the P line is higher (in absolute value) than that on the O lines, the enrichment is more important on the P line whatever c_{bulk}. As suspected, due to the strong repulsive interaction between the O lines, the O lines split into two groups (within a range of temperature and concentration): rich and poor lines. The separation of one isotherm in two isotherms is the signature of an order-disorder transition.

To obtain the phase diagram associated to this transition, we calculate the isotherms at various temperatures. Fig. 3a shows the isotherms as a higher temperature ($T = 5000$ K). We can note that this temperature is higher than the melting temperature which is about 3700 K. Above the melting temperature, the results obtained on a rigid lattice are purely theoretical, but allow to describe the thermal decreasing of segregation and ordering. As the temperature is increased (but still below the order-disorder temperature), the isotherms on the different lines are shifted to higher bulk concentrations, the slope of the isotherms and the enrichment factor c_X/c_{bulk} decrease. The transition that is characterized by the separation of the O lines into two groups is bounded at a given temperature in a bulk concentration range $c_{bulk} \in [c_{b1}, c_{b2}]$ and in an O line concentration range by the solubility limits c_α and c_β (see Fig. 3a). Note that in this domain, the average O isotherm $\langle c_O \rangle$ is a monotonic increasing function.

As the temperature increases, these limits decrease (see Figs. 3b and 3c). Fig. 3b displays the diagram of existence of order (c_{bulk}, T). The diagram is asymmetric, the limit c_{b1} varies little while c_{b2} varies a lot with temperature. For a bulk concentration c_{bulk} between c_{b1} and c_{b2} the structure is ordered with a carbon-rich O_1 line and a carbon-poor O_2 line whose respective concentrations are given by the isotherms for the c_{bulk} value. The phase diagram of O-lines $(\langle c_O \rangle, T)$ is more symmetric (Fig. 3c). For an average concentration $\langle c_O \rangle$ of the O lines between c_α and c_β the composition of each line is given by the isotherms at the horizontal of $\langle c_O \rangle$.

As the temperature decreases, the isotherm c_1 of the rich O line presents a van der Waals loop, indicating a first order intra-line transition (see Fig. 4a). This demixtion-disorder transition is due to the attractive interaction between carbon-carbon atoms on the same O line. We can use the rule of equal areas to obtain the solubility limits. This

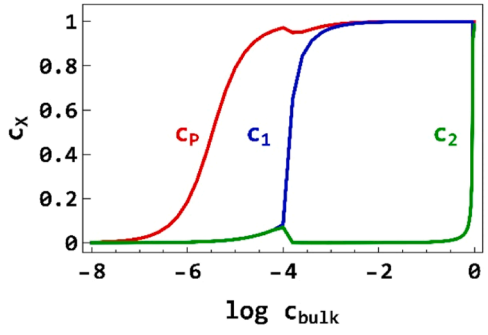

Fig. 2. Equilibrium segregation isotherms for the prismatic P line (in red) and for the octahedral O_1 (in blue) and O_2 (in green) lines of the screw dislocation at T = 2000 K. (For interpretation of the references to colour in this figure legend, the reader is referred to the web version of this article.)

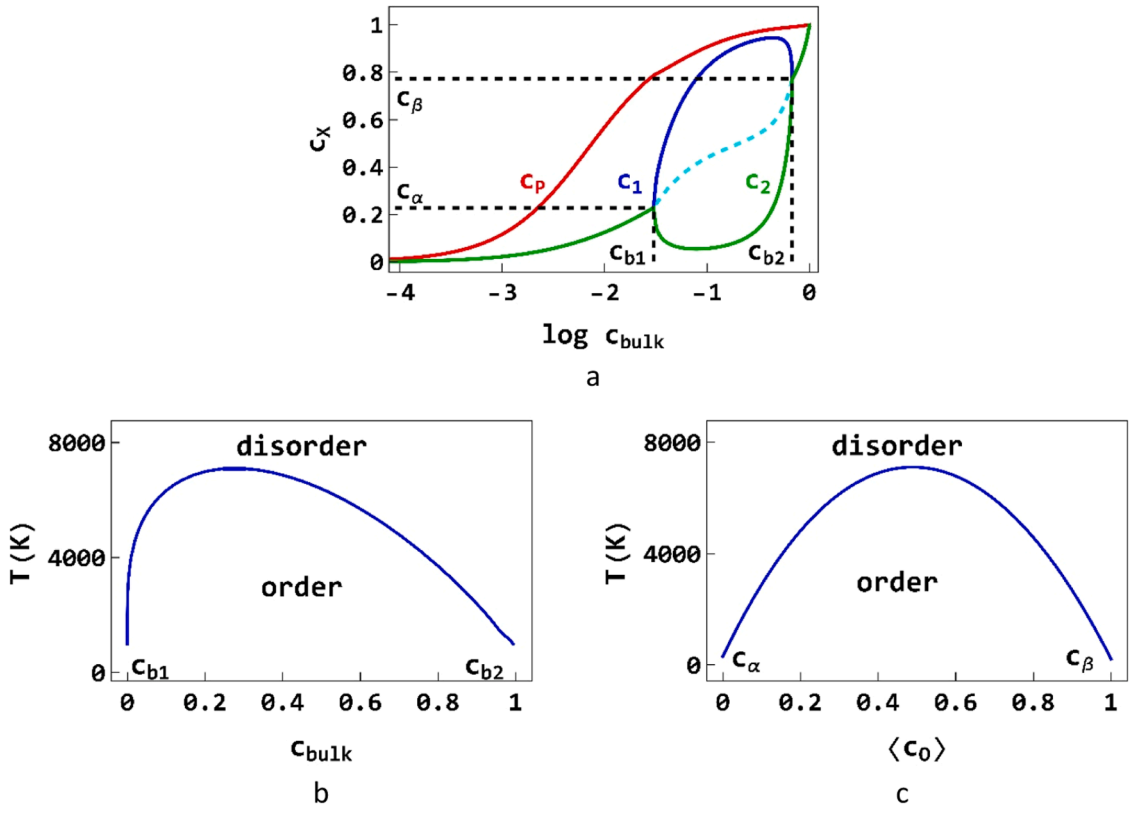

Fig. 3. Equilibrium segregation isotherms for the prismatic P line (in red) and for the octahedral O_1 (in blue), O_2 (in green) lines and for the average isotherm of O lines (in cyan) of the screw dislocation at T = 5000 K (a), domain of existence of the ordered states in c_{bulk} (b), phase diagram of ordered state in $\langle c_O \rangle$ (c). (For interpretation of the references to colour in this figure legend, the reader is referred to the web version of this article.)

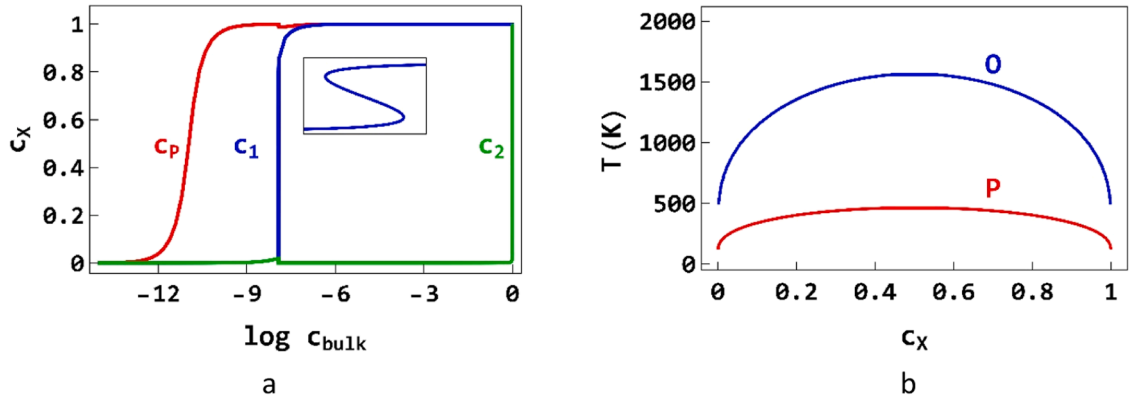

Fig. 4. Equilibrium segregation isotherms for the prismatic P line (in red) and for the octahedral O_1 (in blue) and O_2 (in green) lines of the screw dislocation at T = 1000 K (a) and intra-lines phase diagram P and O (b). (For interpretation of the references to colour in this figure legend, the reader is referred to the web version of this article.)

rule ensures that the two phases, one rich and the other one poor in carbon, have the same free energy. The isotherm of line *P* shows the same behavior at lower temperatures. The intra-*O* critical temperature T_c^O, below which a first order phase transition is observed on the *O* line, is slightly less than 1600 K. The same consideration for the c_P curve leads to an estimation of T_c^P about 500 K. The demixtion-disorder critical temperature for the *O* lines is higher than that for the *P* line. The intra-line phase diagrams, obtained by drawing the solubility limits, present a miscibility gap (see Fig. 4b).

The intra-line critical temperatures given by $T_c^X = -\frac{Z}{4}\frac{V_{XX}}{k_B}$ in the mean-field approximation are overestimated compared to the exact MC calculation. For a one-dimensional system, the critical temperature is expected to be 0 in the MC method. The signature of the phase transition should be characterized by a strong local homoatomic order along these lines.

To summarize the main thermodynamic properties of the three lines model, note that

- there are two transitions which affect the lines *O*: one order-disorder transition (related to the repulsive interactions between lines *O*), and one demixtion-disorder transition (related to the attractive intra-line interactions *O*) leading to the phase diagram in c_{bulk} and *T* (Fig. 3b) or, easier to draw, in c_O and *T* (Fig. 4c). These transitions have almost no effect on the *P* line.

- there is a demixtion-disorder transition affecting the *P*-line related to the weak attractive interactions V_{PP} on the *P*-line leading to a critical mean field temperature close to 500 K. Phase separation on the *P*-line occurs at low temperatures and at very low bulk concentration (of about 10^{-28}).

4.2. Isoconcentrations

The evolution of the concentration profile as a function of temperature is shown Fig. 5a for c_{nom} equal to 10 and 100 appm. The *P* line is fully saturated in carbon atoms at low temperatures up to about 2000 K for these nominal concentrations. Then when the temperature increases the concentration decreases. For *O* lines, we obtain a behavior very different without the constraint imposing that all the lines *O* have identical behavior, than the one observed with this constraint (as in the original paper [33]). The strong repulsive inter-*O*-lines interaction leads to an order-disorder transition at low temperatures which is characterized by a separation in two groups of the *O* lines, one rich and the other poor in carbon. This yields more classical result with line concentrations equal to 1 or 0 when $T\rightarrow 0$ K (Fig. 5a).

The temperature T_m^X at which the concentration of the line *X* is equal to $c_X = 0.5$ can easily be calculated by assuming that the lines are independent. The system is thus reduced to a single equation that describes the evolution of c_X with temperature $\frac{c_X}{1-c_X} = \frac{c_{bulk}}{1-c_{bulk}} exp\left(-\frac{\Delta E_X^{seg}}{k_B T}\right)$ and $c_{bulk} = c_{nom}/3$. To obtain the expression of T_m^X additional assumptions are required:

- $c_1 = c_2 = 0$ for the *P* line. We then obtain the following expression $T_m^P = (\Delta E_P^{seg,0} + V_{PP})/k_B \ln\frac{c_{bulk}}{1-c_{bulk}}$. This formula leads to $T_m^P = 2451$ K for $c_{nom} = 100$ appm and $T_m^P = 2003$ K for $c_{nom} = 10$ appm.
- $c_0 = 1$ and $c_2 = 0$ for the O_1 line rich in carbon. T_m^O is then given by $T_m^O = (\Delta E_O^{seg,0} + 2\,V_{PO} + V_{OO})/k_B ln\frac{c_{bulk}}{1-c_{bulk}}$ which yields $T_m^O = 1720$ K for $c_{nom} = 100$ appm and $T_m^O = 1406$ K for $c_{nom} = 10$ appm.

This simplified model gives values in perfect agreement with full calculations (Fig. 5a).

Fig. 5b compares the evolution of the temperatures T_m^P and T_m^O as a function of the nominal concentration with the critical temperatures T_c^P and T_c^O. If $T_m^P > T_c^P$ whatever c_{nom}, T_m^O is lower than T_c^O when c_{nom} is lower than 36 appm. When $T_m^O < T_c^O$ for a given value of c_{nom}, the concentration for the *O* line rich in carbon c_1 exhibits a jump due to the intra-line phase transition (see Fig. 5a for $c_{nom} = 10$ appm).

To illustrate the influence of the ordering phenomena on the carbon segregation we compare the isoconcentrations obtained in MF when chemical order is taken into account [Eqs. (5-6)] or not, *i.e.* from a two-equation model, that assums that all *O* lines have the same composition. For the current model, we calculate the average composition of the two *O* lines ($\langle c_O\rangle = (c_1 + c_2)/2$). The comparison is shown at $c_{nom} = 100$ appm in Fig. 6. The isoconcentration of the *P* line obtained with both approaches are identical (Fig. 6). The average curve of the *O* lines differs strongly from the curve derived from the two-equation model. When $T\rightarrow 0$ K the average concentration is therefore ½ which is quite different from $c_O \approx 0.9$ obtained with the two-equation model.

At low temperatures, the strong inter-*O*-line interaction lead to an ordered equilibrium state with one *O* line rich and the other poor in carbon. Hence the disordered state considered in the two-equation model is unstable. This artificial convergence toward $c_O \approx 0.9$ when $T\rightarrow 0$ K corresponds to the cancellation of the exponential argument in the fundamental segregation equation in the disordered state:

$$-k_B T\ ln\left(\frac{c_O}{1-c_O}\right) + k_B T\ ln\left(\frac{c_{bulk}}{1-c_{bulk}}\right) = \Delta E_O^{seg,0} + 2V_{PO}c_P + V_{OO}c_O \qquad (7)$$

With $V_{OO} = 2V_{OO} + V_1 + 2V_2 + V_3 + 2V_4 = 1.37$ eV.

When $T\rightarrow 0$ K the left-hand side of Eq. (7) tends to 0 and $c_P = 1$. So, the right-hand side of Eq. (7) becomes $\Delta E_O^{seg,0} + 2V_{PO} + V_{OO}\ c_O = 0$, which results in $c_O = 0.92$.

This result explains why, in the two-equation model, all curves of c_O converge to 0.92 when $T\rightarrow 0$ K, whatever the nominal concentration. This is a nice artifact of the two-equation model. The segregation

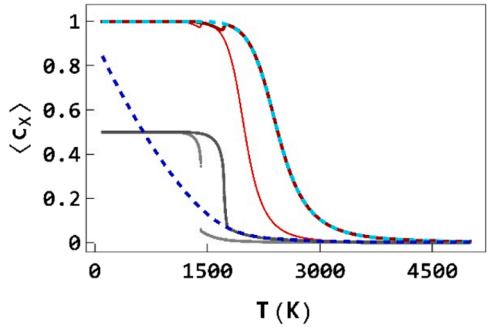

Fig. 6. Evolution of c_P (in red), $\langle c_O\rangle = (c_1 + c_2)/2$ (in gray) concentrations with respect to the temperature for $c_{nom} = 10$ (light) and 100 (dark) appm, comparison with isoconcentrations issued from the model with only two equations for $c_{nom} = 100$ appm (dashed lines, in cyan for P and blue for O). (For interpretation of the references to colour in this figure legend, the reader is referred to the web version of this article.)

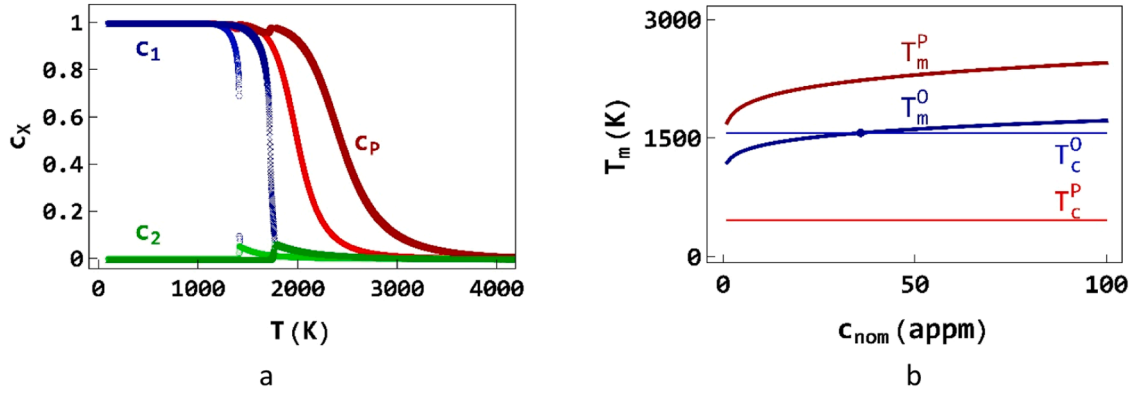

Fig. 5. Evolution of c_P (in red), c_1 (in blue) and c_2 (in green) concentrations with respect to the temperature for $c_{nom} = 10$ (light circles) and 100 (dark crosses) appm (a), Evolution of the temperature corresponding to $c_X = 0.5$, with X = P : T_m^P (dark red) and X = O : T_m^O (dark blue) as a function of the nominal concentration, critical temperatures of the P line (in red) and O line (in blue) are recalled (b). (For interpretation of the references to colour in this figure legend, the reader is referred to the web version of this article.)

enthalpy must cancel for some value of c_O, which requires an interaction term involving c_O. An interaction term means an ordered structure (or demixing) at 0 K. This shows the inadequacy of a model imposing a disordered state.

4.3. Monte Carlo results

In this section, we compare the MC isoconcentrations with the mean-field ones. Fig. 7 shows that isoconcentrations are very similar. This result validates the accuracy of the three-equation MF model. However, we can note that the MC curve of the *O*-line rich in carbon O_1 is slightly shifted toward a lower temperature when compared with the MF curve (see Fig. 7).

With MC simulations, a concentration jump like the one in the MF formalism is not expected because the dislocation is almost a one-dimensional system. For a one-dimensional system, the critical temperature is zero in MC, there is no phase separation [53]. However, the alloy tendency can be characterized by the short-range order parameter defined by Eq. (4). A random solid solution is characterized by $\alpha_{XY} = 0$, for an ordered configuration $\alpha_{XY} < 0$, whereas $\alpha_{XY} > 0$ indicates a tendency to form homoatomic bonds with $\alpha_{XY} = 1$ for perfect two-block phase separation.

Fig. 7a depicts the evolution of intra-line SRO parameter as a function of the temperature. The curves of line *P* and the two *O* lines show a positive peak characteristic of a tendency to phase separation. The peak of the prismatic line occurs around 2500 K. The value of α_{P-P} is very small because the intra-line interaction energy *P* is weak. For the octahedral lines the value of the SRO parameter at the peak (for *T* about 1600 K) is higher ($|V_{OO}| > |V_{PP}|$) showing a higher tendency to form homoatomic bonds. The LRO parameter inter *O*-lines is equal to −1 at low temperature and to 0 at high temperature (Fig. 7b). This is the signature of a perfect ordered state which evolves toward a disordered solution when the temperature increases.

To conclude, for MC simulations, the order-disorder transition is present but the demixtion-disorder transition disappears as expected for one-dimensional systems.

4.4. Influence of the dislocation density

Isotherms and isoconcentrations can be easily obtained as a function of the nominal concentration from the previous results and from the matter conservation (Eq. 7). When the dislocation density increases the number of segregation sites increases thus the segregation can be limited to respect the matter conservation. The influence of the dislocation density is shown on the isoconcentrations for $c_{nom} = 100$ appm (Fig. 8a) and $c_{nom} = 10$ appm (Figs. 8b and 8c). At $c_{nom} = 100$ appm, the composition of the dislocation is identical than for the isolated dislocation whatever the temperature for $\rho = 10^{13}$ m^{-2} and $\rho = 10^{14}$ m^{-2}. For $\rho = 10^{15}$ m^{-2} the segregation is limited on the octahedral lines rich in carbon and the *P*-curve is slightly shifted towards the lower temperatures (Fig. 8a). At a lower nominal concentration, $c_{nom} = 10$ appm, the isoconcentrations are unchanged at $\rho = 10^{13}$ m^{-2}. At higher dislocation density the segregation is limited (Figs. 8b and 8c). For $\rho = 10^{14}$ m^{-2} the same profile as above (for $c_{nom} = 100$ appm and $\rho = 10^{15}$ m^{-2} see Fig. 8a) is observed. As the dislocation density increases, for $\rho = 10^{15}$ m^{-2}, the concentration of all octahedral lines is zero at any temperature and the concentration of prismatic sites is limited to about 0.2 at low temperatures (Fig. 8c).

The influence of dislocation density on the isoconcentrations can be easily dealt in the disordered state by considering Eq. (7) and the isoconcentrations of the dislocation alone. From the profile we assume that $c_2 = 0$ for three octahedral lines and that c_{bulk} is negligible. Thus, Eq. 7 can be rewritten as $c_{nom} = 3\rho\frac{a^3}{6b}(c_P + 3c_1)$. From this relationship we

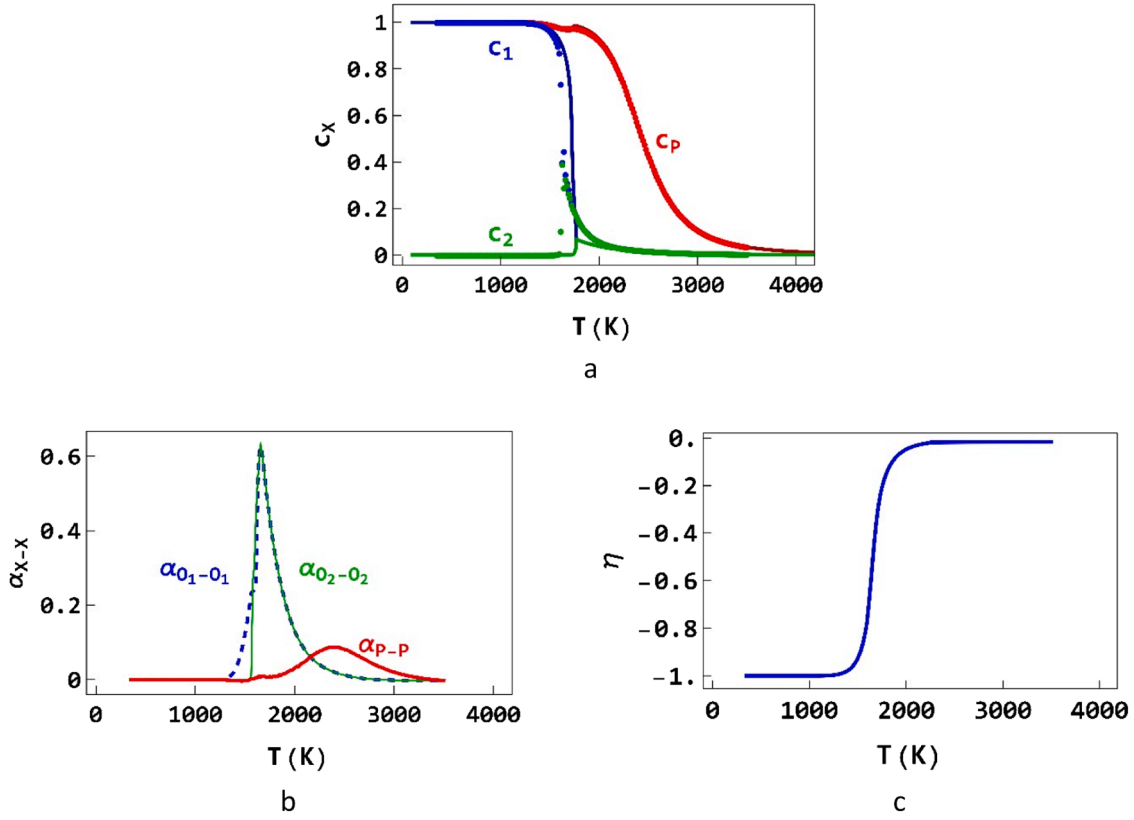

Fig. 7. Comparison between MC (symbols) and MF isoconcentrations (lines) for $c_{nom} = 100$ appm (a). Evolution as a function of the temperature of the MC intra-line short range order parameter (b) and of the MC inter-line long range order parameter η (c). (a and b) P (in red), O_1 (in blue) and O_2 (in green). (For interpretation of the references to colour in this figure legend, the reader is referred to the web version of this article.)

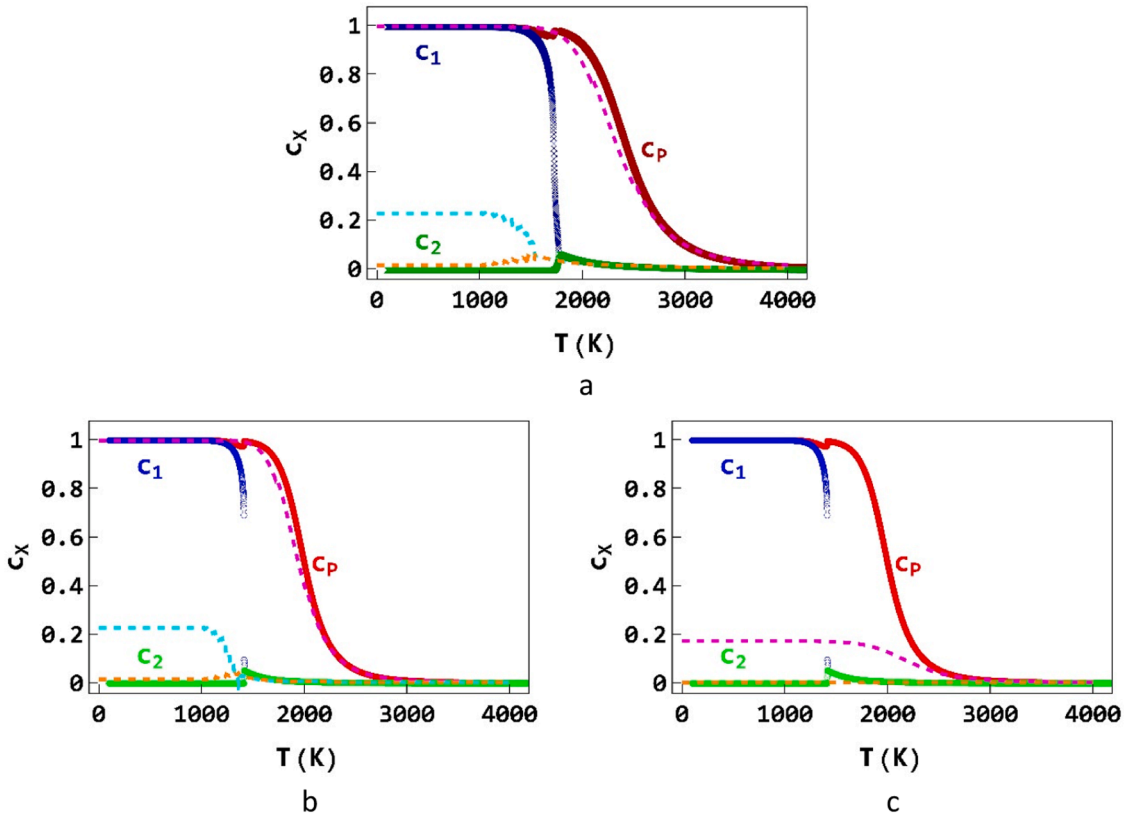

Fig. 8. Influence of the dislocation density on the isoconcentrations for $c_{nom} = 100$ appm and $\rho = 10^{15}$ m^{-2} (a), $c_{nom} = 10$ appm and $\rho = 10^{14}$ m^{-2} (b), $c_{nom} = 10$ appm and $\rho = 10^{15}$ m^{-2} (c). (a-c) single dislocation : red for P, blue for O_1 and green for O_2, and dashed lines for ρ: pink for P, cyan for O_1 and orange for O_2. For $c_{nom} = 100$ appm, profiles are identical to the single dislocation for $\rho < 10^{15}$ m^{-2} (not drawn). For $c_{nom} = 10$ appm, profiles are identical for $\rho = 10^{14}$ m^{-2} and $\rho = 10^{13}$ m^{-2} (not drawn). (For interpretation of the references to colour in this figure legend, the reader is referred to the web version of this article.)

calculate

- the value of ρ from which the segregation is limited by the dislocation density. For $c_P = c_1 = 1$ the right-hand side term is about $10^{-19}\rho$. By writing $c_{nom} = 10^{-n}$, the dislocation density starts to restrict segregation for $\rho > 10^{19-n}$, *i.e.* 10^{15} for $c_{nom} = 10^{-4}$ (100 appm) and $\rho > 10^{14}$ for $c_{nom} = 10^{-5}$ (10 appm).
- the value of c_1 when the segregation is limited on the O_1-line. c_1 is given by $c_1 = \left(\frac{2}{\rho a^3}\ c_{nom} - c_P\right)/3$ with $c_P = 1$, resulting in $c_1 = 0.24$. This result is very different from the one obtained with a two-equation model.
- the value of c_P when the segregation is limited on the *P*-line. All *O*-lines are empty and $c_P = \frac{2}{\rho a^3}\ c_{nom} = 0.17$.

All these results are in perfect agreement with the full calculation.

5. Discussion

In this paper, we have investigated the segregation of carbon atoms in screw dislocations of tungsten using a MF model and MC simulations. The mean field model describes the behavior of the prismatic line and two octahedral lines to observe a hypothetical ordered state. This MF model predicts an intra *P*-line transition at low temperatures for negligible bulk concentrations, so experimental evidence should not be possible. At low temperatures the sites of the prismatic line are occupied by carbon atoms. From about 2200 K the carbon concentration of the prismatic line decreases with increasing temperature (for $c_{nom} = 100$ appm). The behavior of the octahedral lines is more complex. We find, at low temperatures, that one octahedral line is saturated in carbon atoms and the other without any, forming an alternative sequence. The concentration of carbon of the rich *O*-line decreases from 1700 K (for $c_{nom} = 100$ appm). In addition, at temperatures up to 1600 K, an intra-line demixing/disordering transition occurs. This transition is characterized by a concentration jump on the isoconcentration curves when the nominal concentration is below 36 appm.

Our mean field results are very different from those obtained with a model that assumes that all *O*-lines have identical behavior. The temperatures for which the *P*-line is predicted to be saturated with carbon and all *O*-lines are empty are between 1800 K and 2300 K. At lower temperatures three of the six *O*-lines are rich in carbon.

MC simulations show that order-disorder transition between *O*-lines occurs while the demixtion-disorder transitions along the lines disappear as the system is almost one-dimensional. The presence of attractive interactions is only depicted by the existence of atomic and vacancy clusters. The MC microstructures present at low temperatures the ordered state with rich and poor *O*-lines (Fig. 9a). When the temperature increases and the concentration of carbon-rich *O*-lines decreases (Fig. 7a), clusters of vacancies appear on the carbon-rich *O*-lines (Fig. 9b). For higher temperatures, when the concentration of carbon rich *O*-lines decreases further and the concentration of carbon-poor *O*-lines increases a little (Fig. 7a), the microstructures reveal the presence of carbon clusters on the carbon-poor *O*-lines, these clusters are opposite to vacancy clusters on the carbon-rich *O*-lines (Fig. 9c). These microstructures show the formation of local anti-phase boundaries (LAPBs). Each LAPB is restricted to a given pair of *O*-lines. Actually, each pair being independent of the other two, the LAPBs for a pair of *O*-lines are not correlated with the LAPBs located on the other two pairs, preventing us to define a global APB perpendicular to the dislocation line and affecting the three pairs of *O*-lines. The presence of vacancy clusters or carbon clusters on the *O*-lines is in accordance with the description of

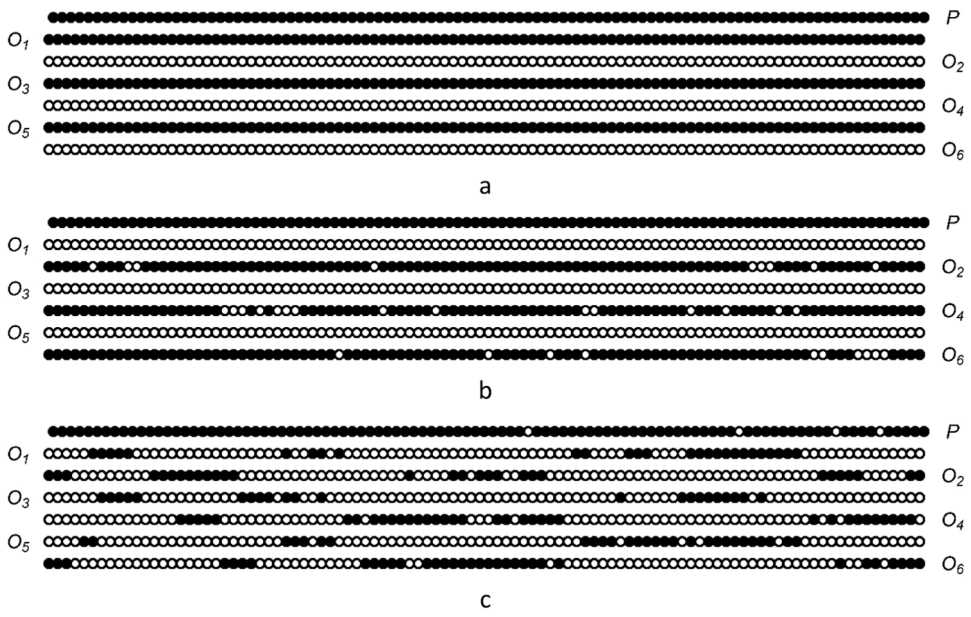

Fig. 9. Monte Carlo microstructures obtained for a single dislocation for c_{nom} = 100 appm at T = 1280 K (a), T = 1595 K (b), T = 1673 K (c). Circles: empty sites, black disk: carbon atoms. (For interpretation of the references to colour in this figure legend, the reader is referred to the web version of this article.)

the local order presented previously.

Segregation on dislocations leads to a wide variety of phenomena. Many improvements in microscopy have been made and allowing the imaging of light atoms [57], but it remains an open question whether it is possible to see the ordering in the dislocation. Our results illustrate the complexity when two phase transitions intertwine. This complexity cannot always be described by the simplest mean field models. The choice of the model depends directly on the complexity of the system. The comparison with MC simulations allows to validate the relevance of the chosen model.

6. Conclusion

The effect of chemical ordering phenomena on carbon segregation in tungsten screw dislocation changes drastically the concentration of solutes atoms in the dislocation and the microstructures. If the carbon concentration of prismatic sites remains unchanged, the carbon concentration of octahedral sites presents a large athermal plateau and phase transitions appear that induce abrupt variations of the concentration. This is an important result for future studies of the mobility of screw dislocations in W(C). For instance, in the temperature range where carbon atoms are mobile (above 1373 K) and segregate in the dislocations, the configuration which has to be considered is a prismatic line saturated in carbon atoms and ordered octahedral lines of average equiatomic composition up to 1500 K for c_{nom} = 10 appm and 1700 K for c_{nom} = 100 appm.

Declaration of Competing Interest

The authors declare that they have no known competing financial interests or personal relationships that could have appeared to influence the work reported in this paper.

Acknowledgments

We thank L. Ventelon for giving us the opportunity to study the segregation on dislocations, and R. Tétot and D. Bérardan for their critical reading and helpful discussions.

References

[1] L. Zou, C. Yang, Y. Lei, D. Zakharov, J.M.K. Wiezorek, D. Su, Q. Yin, J. Li, Z. Liu, E. A. Stach, J.C. Yang, L. Qi, G. Wang, G. Zhou, Dislocation nucleation facilitated by atomic segregation, Nat. Mater. 17 (2018) 56–63, https://doi.org/10.1038/nmat5034.

[2] Y. Kuk, P.J. Silverman, T.M. Buck, Structure of segregated Au layers on Ni(110) –0.8 at. % Au alloy by scanning tunneling microscopy, Phys. Rev. B. 36 (1987) 3104–3107, https://doi.org/10.1103/PhysRevB.36.3104.

[3] M. Schmid, H. Stadler, P. Varga, Direct observation of surface chemical order by scanning tunneling microscopy, Phys. Rev. Lett. 70 (1993) 1441–1444, https://doi.org/10.1103/PhysRevLett.70.1441.

[4] K.L. Merkle, High-resolution electron microscopy of interfaces in FCC materials, Ultramicroscopy 37 (1991) 130–152, https://doi.org/10.1016/0304-3991(91)90013-V.

[5] T.T. Tsong, Atom-probe field ion microscopy and applications to surface science, Surf. Sci. 299–300 (1994) 153–169, https://doi.org/10.1016/0039-6028(94)90652-1.

[6] D. Blavette, A. Bostel, J.M. Sarrau, B. Deconihout, A. Menand, An atom probe for three-dimensional tomography, Nature 363 (1993) 432–435, https://doi.org/10.1038/363432a0.

[7] M.K. Miller, Atom probe tomography characterization of solute segregation to dislocations and interfaces, J. Mater. Sci. 41 (2006) 7808–7813, https://doi.org/10.1007/s10853-006-0518-5.

[8] S. Piazolo, A. La Fontaine, P. Trimby, S. Harley, L. Yang, R. Armstrong, J. M. Cairney, Deformation-induced trace element redistribution in zircon revealed using atom probe tomography, Nat. Commun. 7 (2016) 10490, https://doi.org/10.1038/ncomms10490.

[9] G. Tréglia, B. Legrand, F. Ducastelle, Segregation and ordering at surfaces of transition metal alloys: the tight-binding ising model, Europhys. Lett. 7 (1988) 575–580, https://doi.org/10.1209/0295-5075/7/7/001.

[10] I. Meunier, G. Tréglia, R. Tétot, J. Creuze, F. Berthier, B. Legrand, Misfit dislocation loops or incommensurate structure at an interface: vibrational and anharmonic effects, Phys. Rev. B. 66 (2002), 125409, https://doi.org/10.1103/PhysRevB.66.125409.

[11] R. Tétot, F. Berthier, J. Creuze, I. Meunier, G. Tréglia, B. Legrand, Cu-ag (111) polymorphism induced by segregation and advacancies, Phys. Rev. Lett. 91 (2003) 1–4, https://doi.org/10.1103/PhysRevLett.91.176103.

[12] J. Creuze, F. Berthier, R. Tétot, B. Legrand, Phase transition induced by superficial segregation: the respective role of the size mismatch and of the chemistry, Surf. Sci. 491 (2001) 1–16, https://doi.org/10.1016/S0039-6028(01)01429-7.

[13] D.N. Seidman, B.W. Krakauer, D. Udler, Atomic scale studies of solute-atom segregation at grain boundaries: experiments and simulations, J. Phys. Chem. Solids. 55 (1994) 1035–1057, https://doi.org/10.1016/0022-3697(94)90123-6.

[14] J.D. Rittner, D.N. Seidman, Solute-atom segregation to ⟨110⟩ symmetric tilt grain boundaries, Acta Mater 45 (1997) 3191–3202, https://doi.org/10.1016/S1359-6454(97)00002-5.

[15] F. Berthier, B. Legrand, G. Tréglia, How to compare superficial and intergranular segregation? A new analysis within the mixed SMA–TBIM approach, Acta Mater 47 (1999) 2705–2715, https://doi.org/10.1016/S1359-6454(99)00144-5.

[16] J. Creuze, F. Berthier, R. Tétot, B. Legrand, Wetting and structural transition induced by segregation at grain boundaries: a Monte Carlo study, Phys. Rev. Lett. 86 (2001) 5735–5738, https://doi.org/10.1103/PhysRevLett.86.5735.
[17] G. Rossi, R. Ferrando, C. Mottet, Structure and chemical ordering in CoPt nanoalloys, Faraday Discuss 138 (2008) 193–210, https://doi.org/10.1039/B705415G.
[18] D. Cheng, S. Yuan, R. Ferrando, Structure, chemical ordering and thermal stability of Pt-Ni alloy nanoclusters, J. Phys. Condens. Matter. (2013) 25, https://doi.org/10.1088/0953-8984/25/35/355008.
[19] F. Lequien, J. Creuze, F. Berthier, B. Legrand, Superficial segregation in nanoparticles: from facets to infinite surfaces, J. Chem. Phys. 125 (2006), 094707, https://doi.org/10.1063/1.2245804.
[20] F. Lequien, J. Creuze, F. Berthier, I. Braems, B. Legrand, Superficial segregation, wetting, and dynamical equilibrium in bimetallic clusters: A Monte Carlo study, Phys. Rev. B. 78 (2008), 075414, https://doi.org/10.1103/PhysRevB.78.075414.
[21] V. Moreno, J. Creuze, F. Berthier, C. Mottet, G. Tréglia, B. Legrand, Site segregation in size-mismatched nanoalloys: application to Cu–Ag, Surf. Sci. 600 (2006) 5011–5020, https://doi.org/10.1016/j.susc.2006.08.030.
[22] E. Maras, F. Berthier, B. Legrand, Stability diagram of janus and core–shell configurations in bimetallic nanowires, J. Phys. Chem. C. 120 (2016) 22670–22680, https://doi.org/10.1021/acs.jpcc.6b06707.
[23] A.H. Cottrell, B.A. Bilby, Dislocation theory of yielding and strain ageing of iron, Proc. Phys. Soc. Sect. A. 62 (1949) 49–62, https://doi.org/10.1088/0370-1298/62/1/308.
[24] I. Medouni, A. Portavoce, P. Maugis, P. Eyméoud, M. Yescas, K. Hoummada, Role of dislocation elastic field on impurity segregation in Fe-based alloys, Sci. Rep. 11 (2021) 1780, https://doi.org/10.1038/s41598-020-80140-4.
[25] E. Clouet, S. Garruchet, H. Nguyen, M. Perez, C.S. Becquart, Dislocation interaction with C in α-Fe: a comparison between atomic simulations and elasticity theory, Acta Mater 56 (2008) 3450–3460, https://doi.org/10.1016/j.actamat.2008.03.024.
[26] W. Cai, R.B. Sills, D.M. Barnett, W.D. Nix, Modeling a distribution of point defects as misfitting inclusions in stressed solids, J. Mech. Phys. Solids. 66 (2014) 154–171, https://doi.org/10.1016/j.jmps.2014.01.015.
[27] Y. Gu, J.A. El-Awady, Theoretical framework for predicting solute concentrations and solute-induced stresses in finite volumes with arbitrary elastic fields, Mater. Theory. 4 (2020) 1, https://doi.org/10.1186/s41313-020-00020-2.
[28] E.E. Zhurkin, D. Terentyev, M. Hou, L. Malerba, G. Bonny, Metropolis Monte-Carlo simulation of segregation in Fe–Cr alloys, J. Nucl. Mater. 417 (2011) 1082–1085, https://doi.org/10.1016/j.jnucmat.2010.12.191.
[29] H. Ganesan, M. Longsworth, G. Sutmann, Parallel hybrid Monte Carlo /molecular statics for simulation of solute segregation in solids, J. Phys. Conf. Ser. 1740 (2021), 012001, https://doi.org/10.1088/1742-6596/1740/1/012001.
[30] D. Terentyev, F. Bergner, Y. Osetsky, Cr segregation on dislocation loops enhances hardening in ferritic Fe–Cr alloys, Acta Mater. 61 (2013) 1444–1453, https://doi.org/10.1016/j.actamat.2012.11.021.
[31] R.G.A. Veiga, H. Goldenstein, M. Perez, C.S. Becquart, Monte Carlo and molecular dynamics simulations of screw dislocation locking by Cottrell atmospheres in low carbon Fe–C alloys, Scr. Mater. 108 (2015) 19–22, https://doi.org/10.1016/j.scriptamat.2015.06.012.
[32] B. Lüthi, F. Berthier, L. Ventelon, B. Legrand, D. Rodney, F. Willaime, Ab initio thermodynamics of carbon segregation on dislocation cores in bcc iron, Model. Simul. Mater. Sci. Eng. 27 (2019), 074002, https://doi.org/10.1088/1361-651X/ab28d4.
[33] G. Hachet, L. Ventelon, F. Willaime, E. Clouet, Screw dislocation-carbon interaction in BCC tungsten: an ab initio study, Acta Mater. 200 (2020) 481–489, https://doi.org/10.1016/j.actamat.2020.09.014.
[34] P.P.P.O. Borges, E. Clouet, L. Ventelon, Ab initio investigation of the screw dislocation-hydrogen interaction in bcc tungsten and iron, Acta Mater. 234 (2022), 118048, https://doi.org/10.1016/j.actamat.2022.118048.
[35] C. Wolverton, V. Ozolins, A. Zunger, Short-range-order types in binary alloys: a reflection of coherent phase stability, J. Phys. Condens. Matter. 12 (2000) 2749–2768, https://doi.org/10.1088/0953-8984/12/12/314.
[36] A. Hizi, A. Front, M. Said, F. Berthier, G. Tréglia, C. Mottet, Tight-binding Ising modeling of the interplay between bulk ordering and surface segregation in Pt-Ag nanoalloys, Surf. Sci. 700 (2020), 121626, https://doi.org/10.1016/j.susc.2020.121626.
[37] M. Schmid, P. Varga, Segregation and surface chemical ordering – an experimental view on the atomic scale, Chem. Phys. Solid Surf. (2002) 118–151, https://doi.org/10.1016/S1571-0785(02)80091-8. Elsevier B.V.
[38] G. Tréglia, B. Legrand, F. Ducastelle, A. Saúl, C. Gallis, I. Meunier, C. Mottet, A. Senhaji, Alloy surfaces: segregation, reconstruction and phase transitions, Comput. Mater. Sci. 15 (1999) 196–235, https://doi.org/10.1016/S0927-0256(99)00004-X.
[39] D. Luan, H. Jiang, Theoretical study of surface segregation and ordering in Ni-based bimetallic surface alloys, J. Chem. Phys. 154 (2021), 074702, https://doi.org/10.1063/5.0037913.
[40] R. Tétot, F. Berthier, J. Creuze, I. Meunier, G. Tréglia, B. Legrand, Cu-Ag (111) polymorphism induced by segregation and advacancies, Phys. Rev. Lett. 91 (2003), 176103, https://doi.org/10.1103/PhysRevLett.91.176103.
[41] J. Creuze, F. Berthier, R. Tétot, B. Legrand, Intergranular segregation and ordering effect: a mixed Monte Carlo mean-field approach, Phys. Rev. B. 62 (2000) 2813–2824, https://doi.org/10.1103/PhysRevB.62.2813.
[42] J.D. Rittner, D. Udler, D.N. Seidman, Y. Oh, Atomic scale structural effects on solute-atom segregation at grain boundaries, Phys. Rev. Lett. 74 (1995) 1115–1118, https://doi.org/10.1103/PhysRevLett.74.1115.
[43] R. Ismail, R. Ferrando, R.L. Johnston, Theoretical study of the structures and chemical ordering of palladium–gold nanoalloys supported on MgO(100), J. Phys. Chem. C. 117 (2013) 293–301, https://doi.org/10.1021/jp3093435.
[44] D. Nelli, R. Ferrando, Core–shell vs. multi-shell formation in nanoalloy evolution from disordered configurations, Nanoscale 11 (2019) 13040–13050, https://doi.org/10.1039/C9NR02963J.
[45] J. Tang, L. Deng, S. Xiao, H. Deng, X. Zhang, W. Hu, Chemical ordering and surface segregation in Cu-Pt nanoalloys: the synergetic roles in the formation of multishell structures, J. Phys. Chem. C. 119 (2015) 21515–21527, https://doi.org/10.1021/acs.jpcc.5b06145.
[46] A. Lopes, G. Tréglia, C. Mottet, B. Legrand, Ordering and surface segregation in Co1-cPtc nanoparticles: a theoretical study from surface alloys to nanoalloys, Phys. Rev. B. 91 (2015), 035407, https://doi.org/10.1103/PhysRevB.91.035407.
[47] A. Detor, C. Schuh, Grain boundary segregation, chemical ordering and stability of nanocrystalline alloys: atomistic computer simulations in the Ni–W system, Acta Mater. 55 (2007) 4221–4232, https://doi.org/10.1016/j.actamat.2007.03.024.
[48] O. Kitakami, Y. Shimada, K. Oikawa, H. Daimon, K. Fukamichi, Low-temperature ordering of L10–CoPt thin films promoted by Sn, Pb, Sb, and Bi additives, Appl. Phys. Lett. 78 (2001) 1104–1106, https://doi.org/10.1063/1.1346628.
[49] C.L. Platt, K.W. Wierman, E.B. Svedberg, R. Van De Veerdonk, J.K. Howard, A. G. Roy, D.E. Laughlin, L-1 0 ordering and microstructure of FePt thin films with Cu, Ag, Au additive, J. Appl. Phys. 92 (2002) 6104–6109, https://doi.org/10.1063/1.1516870.
[50] M. Saber, H. Kotan, C.C. Koch, R.O. Scattergood, A predictive model for thermodynamic stability of grain size in nanocrystalline ternary alloys, J. Appl. Phys. 114 (2013), 103510, https://doi.org/10.1063/1.4821040.
[51] L. Vega, H.A. Aleksandrov, R. Farris, A. Bruix, F. Viñes, K.M. Neyman, Chemical ordering in Pt–Au, Pt–Ag and Pt–Cu nanoparticles from density functional calculations using a topological approach, Mater. Adv 2 (2021) 6589–6602, https://doi.org/10.1039/D1MA00529D.
[52] S.M. Kozlov, G. Kovács, R. Ferrando, K.M. Neyman, How to determine accurate chemical ordering in several nanometer large bimetallic crystallites from electronic structure calculations, Chem. Sci. 6 (2015) 3868–3880, https://doi.org/10.1039/C4SC03321C.
[53] F. Ducastelle, Order and Phase Stability in Alloys, North-Holland, Amsterdam, 1991.
[54] F. Berthier, J. Creuze, B. Legrand, Effective site-energy model: A thermodynamic approach applied to size-mismatched alloys, Phys. Rev. B. 95 (2017), 224102, https://doi.org/10.1103/PhysRevB.95.224102.
[55] N. Metropolis, A.W. Rosenbluth, M.N. Rosenbluth, A.H. Teller, E. Teller, Equation of state calculations by fast computing machines, J. Chem. Phys. 21 (1953) 1087–1092, https://doi.org/10.1063/1.1699114.
[56] H.J. Goldschmidt, J.A. Brand, The tungsten-rich region of the system tungsten-carbon, J. Less Common Met. 5 (1963) 181–194, https://doi.org/10.1016/0022-5088(63)90012-2.
[57] S.D. Findlay, N. Shibata, Y. Ikuhara, R. Huang, E. Okunishi, H. Sawada, Y. Kohno, Y. Kondo, Annular bright-field scanning transmission electron microscopy: direct and robust atomic-resolution imaging of light elements in crystalline materials, Micros. Today. 25 (2017) 36–41, https://doi.org/10.1017/S1551929517001006.